Continental Shelf Research 124 (2016) 13–22

Contents lists available at ScienceDirect

Continental Shelf Research

journal homepage: www.elsevier.com/locate/csr

Research papers

# Changes in bay circulation in an evolving multiple inlet system

Mara M. Orescanin [a,b,*], Steve Elgar [a], Britt Raubenheimer [a]

[a] Woods Hole Oceanographic Institution, 266 Woods Hole Rd., Woods Hole, MA 02543, USA
[b] Department of Mechanical Engineering, Massachusetts Institute of Technology, 77 Massachusetts Ave, Cambridge, MA 02139, USA

ARTICLE INFO

*Article history:*
Received 16 June 2015
Received in revised form
8 April 2016
Accepted 9 May 2016
Available online 10 May 2016

*Key words:*
Multiple inlet circulation
Bathymetric evolution
Bottom friction
Tidal distortion

ABSTRACT

Observations and numerical model (ADCIRC) simulations are used to quantify the changes in circulation within the evolving, shallow, two-inlet tidal Katama system, Martha's Vineyard, MA. From 2011 to 2013, Katama Inlet, connecting Katama Bay to the Atlantic, became 5 times longer, 1/3 as wide, and 1/3 as deep as the inlet migrated and rotated. This morphological evolution caused a significant loss of energy throughout Katama Bay and Edgartown Channel, which connects the bay to Vineyard Sound. The decrease in energy as the inlet evolved between 2011 and 2013 was not monotonic. Model simulations suggest bathymetric changes caused by Hurricane Irene (August 2011) resulted in a temporary increase in circulation energy throughout the inlets and bay. Changes in the M4 and M6 tidal constituents, harmonics of the primary M2 tidal forcing, suggest the changes in the observed circulation patterns primarily were owing to changes in friction, and not to changes in advection resulting from the evolving inlet location, orientation, or geometry, consistent with previous results.

© 2016 Elsevier Ltd. All rights reserved.

## 1. Introduction

Multiple tidal inlet systems are common coastal features that have complicated circulation patterns owing to the multiple connections between back bays and open water bodies. These coastal features are critical for ecological health, as well as for economic and recreational activities. Circulation in bays and estuaries depends on many factors, including the geometry of the inlets that connect these systems with the ocean (Aubrey and Speer, 1985; Speer and Aubrey, 1985; Speer, 1991; Friedrichs et al., 1992; van de Kreeke et al., 2008; Brouwer et al., 2013; and many others). Temporal changes in inlet geometry and the resulting changes to the circulation can affect navigability and the transport of nutrients throughout the system. In multiple-inlet systems, changes in the geometry of one inlet can affect the circulation differently than in systems with only one connection to the ocean (van de Kreeke et al., 2008; Brouwer et al., 2013).

The effects of friction and inlet geometry on the amplitude and phase (relative to the driving ocean tide) of sea-level fluctuations in a back basin has been quantified in terms of a nondimensional coefficient of repletion (Keulegan, 1967). Friction and advection are described by nonlinear terms in the equations of motion, and thus introduce overtides (harmonics of tidal constituents) and compound tides (combinations of lower-frequency tidal constituents) (Parker, 1991; Blanton, 2002). Temporal changes in the inlet channel geometry can lead to changes in frictional and advective effects. Thus, changes in inlet geometry can alter the distortion of the nearly sinusoidal ocean tide (Keulegan, 1967; Aubrey and Speer, 1985; Speer and Aubrey, 1985; Dronkers, 1986; Friedrichs and Aubrey, 1988; Speer, 1991; Friedrichs, et al., 1992; Fortunato and Oliveira, 2005; Breaker et al., 2008; Malhadas et al., 2009; Nidzieko, 2010; Nidzieko and Ralston, 2012). Determining the relative influence of friction and advection as the inlet geometry evolves is important for understanding the mechanisms by which inlets close.

Although tidal distortion and circulation in inlet systems have been studied for many years (Keulegan, 1967; Aubrey and Speer, 1985; Speer and Aubrey, 1985; Dronkers, 1986; Speer et al., 1991; Prandle, 1991; Friedrichs et al., 1992; MacCready and Geyer, 2010; Nidzieko, 2010; Nidzieko and Ralston, 2012; Geyer and MacCready, 2014), there are few field studies of the effects of temporally changing inlet geometry in a multi-inlet system. Here, observations obtained over several years in the multi-inlet system of Katama Bay, Martha's Vineyard, MA (Fig. 1) are used to investigate the effects of the relatively rapidly changing Katama Inlet on the circulation and tidal distortion in the bay.

Katama Bay is connected to Vineyard Sound through Edgartown Channel, and to the Atlantic Ocean through Katama Inlet (Fig. 1). Tidal sea-surface elevation fluctuations in Vineyard Sound range from 0.5 (neap tides) to 0.9 m (spring tide), and in the Atlantic from 0.6 to 1.2 m (leading the Vineyard Sound tide by ~3 h). Significant wave heights $H_{sig}$ in Vineyard Sound near the mouth of Edgartown Harbor usually are less than 0.3 m, whereas

* Corresponding author at: Woods Hole Oceanographic Institution, 266 Woods Hole Rd., MS # 12, Woods Hole, MA 02543, USA.
*E-mail address:* mara.orescanin@gmail.com (M.M. Orescanin).

http://dx.doi.org/10.1016/j.csr.2016.05.005
0278-4343/© 2016 Elsevier Ltd. All rights reserved.

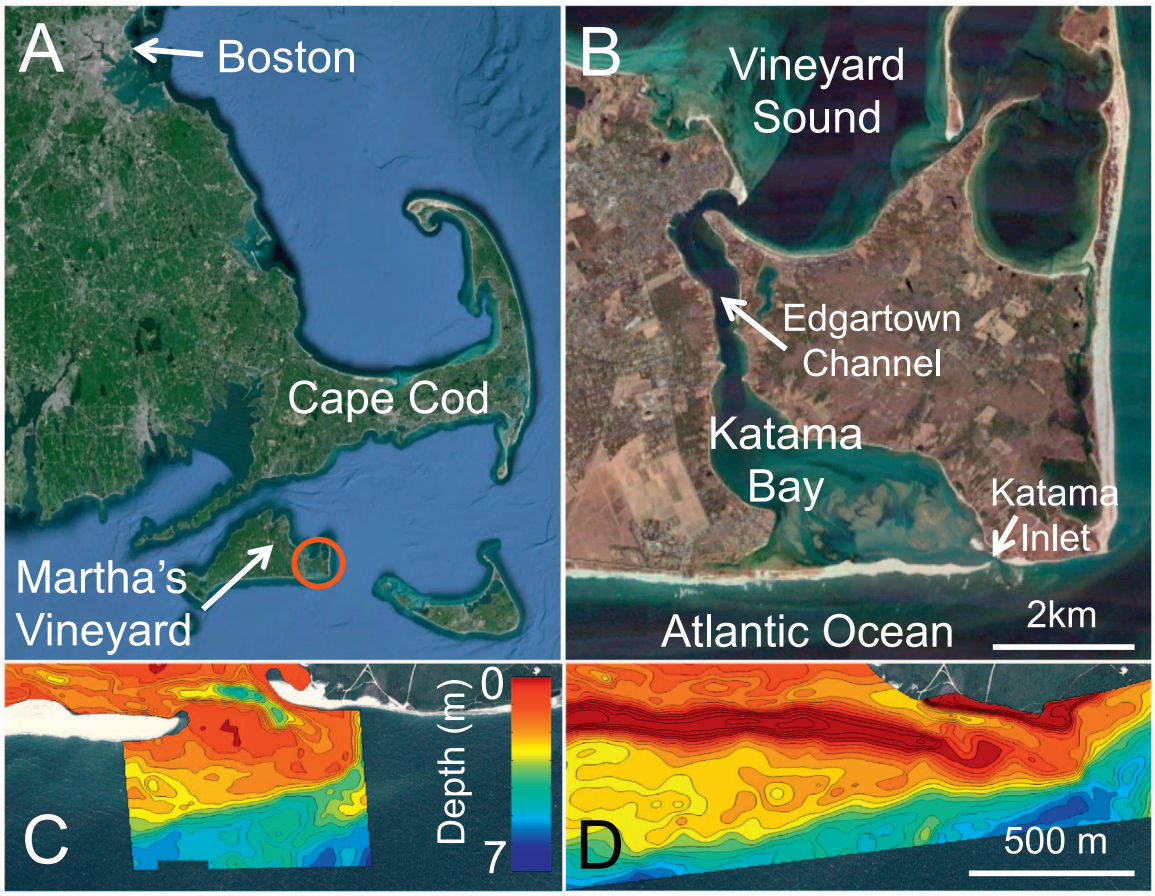


**Fig. 1.** Google Earth images of (A) location of Martha's Vineyard, MA, with the Katama system inside the red circle, and (B) Katama Bay showing Edgartown Channel to the north and Katama Inlet to the south. Bathymetry (color contours, scale on the right) near the mouth of Katama Inlet observed in (C) September 2011 and (D) July 2013 (dark red contours in D are subaerial). The color bar in (C) and the scale bar in (D) apply to both (C) and (D).

significant wave heights in 12-m water depth in the Atlantic near Katama Inlet can be as large as 5 m.

The shoreline along the southern coast of Martha's Vineyard is composed primarily of medium to coarse sand ($0.4 < d_{50} < 0.6$ mm), and the sediments within Katama Bay are finer, with $d_{50}$ ranging from 0.1 to 0.4 mm (Anderson, 2012). Since 2011, Katama Inlet has migrated nearly 1500 m to the east, and its axis has rotated from a nearly N-S orientation to nearly E-W as the sand spit separating the bay from the ocean (Norton Point) has extended eastward and started to wrap around Chappaquiddick Island (Fig. 1(B), (C), (D)). Between 2011 and 2013, the length of Katama Inlet increased from 200 m to nearly 1000 m, the width decreased from 400 m to 150 m, and the depth decreased from 4.0 m to 1.5 m (Fig. 1(C), (D)). Here, the observations are combined with two-dimensional depth-integrated (2DDI) numerical model (ADCIRC) simulations to investigate the effects of the evolving inlet geometry on sea levels and currents within the Katama System, to determine the relative roles of friction and advection, and to quantify the tidal distortion.

## 2. Tidal distortion from friction and changing geometry

Inlets alter the properties of the ocean tide by acting as restrictions to flow from the coastal ocean to the back bay, resulting in modifications to the tidal amplitude and phase, in addition to the generation of overtides and compound tides (Aubrey and Speer, 1985; Friedrichs and Aubrey, 1988; Speer et al., 1991; Friedrichs et al., 1992). Changes in the geometry of an inlet (i. e., physical dimensions and orientation) are well known to alter the sea level and circulation patterns within the inlet and bay, and can alter the role of advection as currents follow different paths (Aubrey and Speer, 1985; Friedrichs and Aubrey, 1988; Speer et al., 1991). Changes in hydraulic radius (cross-sectional area divided by wetted perimeter) and inlet length also can alter the role of friction. For example, as an inlet lengthens, narrows, and shoals, the forcing tides are increasingly restricted, retarding flows into and out of the bay, and thus affecting the circulation within the bay. Both advective and frictional changes affect the propagation of the tide, and in particular generate higher-frequency motions from nonlinear interactions between motions of the primary tidal constituents (Aubrey and Speer, 1985; Speer and Aubrey, 1985; Friedrichs and Aubrey, 1988; Speer et al., 1991; Le Provost, 1991; Parker, 1991; Friedrichs et al., 1992; Blanton, 2002). Assuming a shallow, well-mixed, irrotational system, conservation of mass and momentum in one direction can be expressed as (Parker, 1991):

$$\frac{\partial \eta}{\partial t} = -\frac{\partial}{\partial x}((h+\eta)u) \tag{1}$$

and,

$$\frac{\partial u}{\partial t} + u\frac{\partial u}{\partial x} = -g\frac{\partial \eta}{\partial x} - C_d\frac{1}{h+\eta}u|u| \tag{2}$$

where $\eta$ is the water level relative to mean sea level, $t$ is time, $x$ is the spatial coordinate, $h$ is the mean water depth, $u$ is the depth-averaged velocity, $g$ is gravitational acceleration, and $C_d$ is a drag

coefficient for quadratic friction. To analyze the nonlinear effects of these equations, the friction term can be expanded assuming $\eta^2 \ll h^2$ ($\eta^2 \cong 0.1h^2$ for the shallowest case here, for which the tidal range in the inlet $\eta = 0.5$ m, and the inlet depth $h = 1.5$ m), resulting in:

$$C_d \frac{1}{h+\eta} u|u| \cong \frac{C_d}{h}\left(1 - \frac{\eta}{h}\right) u|u| \tag{3}$$

yielding two separate terms for frictional effects. The absolute value operator results in a doubling of the frequencies of the components of the tidal time series.

The nonlinear terms describing the advection of mass, $\partial(\eta u)/\partial x$, and momentum, $u\partial u/\partial x$, generate even harmonics of the driving motions. For example, advection generates motions primarily at the second harmonic, M4 of an M2 driving tide. Some of the effects of friction, specifically from $-(C_d/h^2)\eta u|u|$, produce even harmonics owing to the absolute value operator. In the absence of a mean current, the lowest even harmonic generated is the 4th harmonic (e.g., M8 is generated from an M2 driving force (Parker, 1991). Usually, owing to the multiplication of decreasingly energetic harmonics, this higher-order interaction is relatively small. In contrast, the other frictional term, $(C_d/h)u|u|$, generates odd harmonics. For example, friction generates motion at M6 from an M2 driving tide.

Thus, even harmonics (e.g., M4) are generated primarily from advection and odd harmonics (e.g., M6) are generated primarily by friction (Parker, 1991; Blanton, 2002; and others). The harmonics can interact with the primary driving tides, as well as with each other, producing higher-frequency motions, such as M6 from the interaction of M2 with its harmonic M4. However, usually these higher-order interactions are relatively small. As the geometry of an inlet system changes in time, the advective distortion and frictional distortion of the tide will change. For a system dominated by the M2 lunar tide, changes in advection should result in a change in energy at the M4 frequency, whereas changes in friction should result in a change in energy at the M6 frequency. Temporal changes in the M4 constituent observed in a one-inlet system have been used to infer changes in bathymetry (Malhadas et al., 2009). Here, observed and modeled M4 and M6 constituents are used to determine the relative roles of advection and friction as the inlet evolves and bay circulation changes.

## 3. Field measurements

The bathymetry from the northern end of Edgartown Channel through Katama Bay and Inlet and across the ebb shoal in the ocean to the south (Figs. 1 and 2) was measured with a GPS- and acoustic-altimeter-equipped personal watercraft. The vertical resolution of the surveys is approximately 0.05 m, and the horizontal resolution is 0.10 m along transects separated by 5 m (near complex bathymetry) to 60 m (uniform bathymetry). Surveys were conducted both before (July 2011, not shown) and after (September 2011, Fig. 1(C)) the passage of Hurricane Irene (29 August 2011)

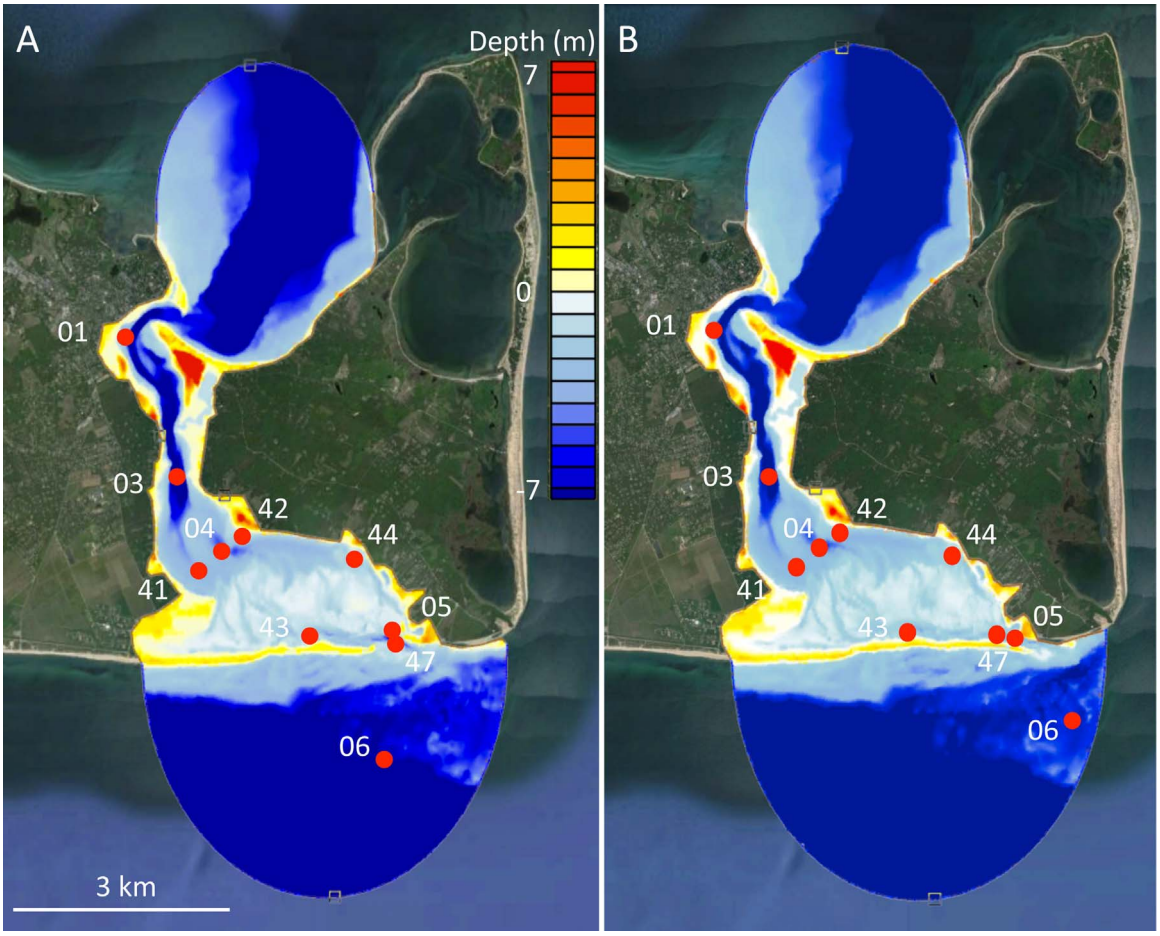


**Fig. 2.** Model domain (color contours are elevation relative to mean sea level) and sensor locations (red symbols) during (A) 2011 and (B) 2013. Sensor 01 is a pressure gauge, sensors 05, 06, and 44 are single point acoustic current meters, and all other sensors are acoustic current profilers. Pressure gauges were colocated with each current meter and profiler. The Martha's Vineyard Coastal Observatory is located about 7 km west of the inlet in 12-m water depth.

and in July 2013 (Fig. 1(D)). The bay surface area is approximately $7.5 \times 10^6$ m$^2$, and water depths range from less than 1 m on the flood shoal to 10 m at the northern part of the Bay (Fig. 2).

In 2011, Katama Inlet was relatively short (200 m), wide (400 m), and deep (4.0 m) and was oriented roughly north-south (Figs. 1(C) and 2(A)). There was a prominent ebb shoal offshore of the inlet mouth, and a large flood shoal intersected by channels on the bay side of the inlet. By 2013, Katama Inlet (and the ebb shoal) had migrated over 1000 m to the east, rotated to a nearly east-west orientation, elongated (1000 m), narrowed (150 m), and shoaled (1.5 m depth) (Figs. 1(D) and 2(B)). By February 2015 the sand barrier separating the bay from the ocean had extended to the eastern edge of Chappaquiddick Island, and the inlet had increased another 700 m in length (not shown). On 1 April 2015, the inlet closed.

Water levels and currents were observed from 1 to 30 September 2011 and from 1 to 26 August 2013. Sea-surface elevation fluctuations were measured (2 Hz samples) with buried pressure gauges deployed along and across the bay and inlets (Fig. 2). The pressure time series were corrected for atmospheric pressure fluctuations. There is an approximately 3-hr phase lag between the M2 tidal constituent in Vineyard Sound and the M2 tide in the ocean (Chen et al., 2011), producing tidally varying pressure gradients from the up to 1-m difference in sea-surface elevation across the 7-km long Katama system, similar to pressure gradients across many inlets.

The pressure gradients drive strong currents, which were measured with profiling acoustic current meters (Fig. 2) and single-point acoustic Doppler velocimeters. The profilers estimated 1-min mean currents in 0.25-m (for sensors in less than 10-m water depth) and 0.50-m ( $>$ 10 m depth) high vertical bins from 0.25 m above the seafloor to the surface (the center of the lowest measurement is $\sim$0.38–0.75 m above the seafloor). Velocimeters were deployed in water too shallow for profilers (sensor 44 in Fig. 2), and on the ebb shoal (sensor 06) and in the inlet (sensor 05) to estimate wave properties (2 Hz samples).

There is no source of fresh water to Katama Bay, and many CTD casts throughout the system showed there was little vertical variation in temperature or salinity (32 PSU). Similarly, there was little vertical variation in measured currents (which were mostly above the boundary layer), and thus depth-averaged 10-min mean velocities are considered here. Wind was measured on the Martha's Vineyard Coastal Observatory (MVCO: http://www.whoi.edu/mvco) 12.5-m-tall meteorological mast on South Beach, Martha's Vineyard, a few km west of Katama Inlet (not shown).

## 4. Model

The numerical hydrodynamic model ADCIRC (Luettich and Westerink, 1991) was implemented for the Katama system. The 2DDI version of ADCIRC solves the continuity and momentum equations, including all nonlinear terms, using finite elements on flexible, unstructured grids that allow for high spatial resolution of spatially varying geometries, such as the complex bathymetry near inlets. In addition, ADCIRC simulates wetting and drying, which can be important to circulation in small bays with tidally varying shorelines owing to the change in bay surface area.

The model bathymetries (Fig. 2) consisted of the watercraft surveys in 2011 and 2013, supplemented with the 2008 Nantucket 10 m resolution DEM (www.ngdc.noaa.gov) in Vineyard Sound and the Atlantic outside the ebb shoal. To account for the effects of wetting and drying, the model requires high-resolution surveys near the shoreline, especially in gently sloping areas where there is significant change during a tidal cycle. In deeper water, especially where the bathymetry is relatively smooth, less dense surveys are sufficient. Model grid resolution was 10 m within Katama Inlet and 30 m elsewhere. Using a 10-m resolution grid everywhere did not change the results.

To keep the model domain small and to compare model results with observations, the simulations are driven at the northern and southern boundaries by the sea-level fluctuations observed in the sound and in the ocean, thus accounting for the complex propagation of tides into the area, as well as the effects of large-scale winds and atmospheric pressure on water levels. The sea levels are applied uniformly at the boundary (boundary normal). Although breaking waves can drive water into the inlet affecting circulation throughout the bay (Malhadas et al., 2009; Wargula et al., 2014; Orescanin et al., 2014), waves were relatively small (in 12 m depth, $0.4 < H_{sig} < 3.2$ m, with $H_{sig} < 1.0$ m 65% of the time) for the data considered here and are not included in the model. Similarly, although the large-scale wind effects on mean water levels are included in the boundary conditions, winds usually were light and the bay surface area is small so local wind stress over the bay is neglected.

In the southern part of the domain, water levels were measured in the ocean (at MVCO), near the boundary (Fig. 2). However, in the northern part of the domain, water levels were measured in Edgartown Harbor (northern-most sensor in Fig. 2), some distance from the boundary in the sound. Thus, to drive the model at the northern boundary the amplitude of the time series of water level observed in Edgartown Harbor (at sensor 01) was increased by 18% so that the simulated water levels in the harbor matched the observed water levels. There was no need to adjust the phase of the Edgartown water levels when applied on the northern boundary.

Using drag coefficients estimated from the observations (Orescanin et al., 2014) at Edgartown Channel ($C_d$=0.007) and Katama Inlet ($C_d$=0.011) and the average water depth over each region, the Manning's $n$ (proportional to $\sqrt{C_d h^{1/3}}$ ) for Edgartown Channel and Katama Bay ($h$=5.0 m) is $n$=0.030 and for Katama Inlet ($h$=1.3 m) is $n$=0.035. In the sound and ocean, $n$=0.020, the value typically used for deeper water. The results are not sensitive to 15% changes in the values of $n$ or to using a spatially constant value of $n$=0.030. However, the spatially variable Manning's $n$ minimizes the overall error in kinetic energy throughout the system. This range in Manning's $n$ values is similar to that used in previous studies of inlets, including multiple tidal inlet systems (Mehta and Joshi, 1988; Friedrichs and Madsen, 1992; Friedrichs, 1995; Kraus and Militello, 1999; Dias et al., 2009).

The model is forced with observed sea-surface elevation time series on the boundaries, and is run with a 0.5 s time step for numerical stability, with a one-day spin up from the initial boundary conditions and an initial flat sea surface over the entire domain. Lateral viscosity is set to 2.0 m$^2$/s. Here, snapshots every 20 min of model simulations of sea-surface elevation and depth-averaged velocities are compared with 20-min averages of observed sea-surface elevation and depth-averaged velocities. Other averaging schemes did not change the results.

## 5. Model-data comparisons

The model simulates the sea-surface elevation fluctuations observed in Katama Inlet with model-data errors less than about 10% (Table 1). In both 2011 (Fig. 3(A)) and 2013 (Fig. 3(D)) sea level is predicted accurately during spring and neap tides. The (relatively small) model errors during neap tide 16–18 Sep 2011 (Fig. 3(A)) could be caused by neglect of the effects of 3-m high offshore (12-m water depth) waves during a nor'easter storm that peaked on 16 Sep.

**Table 1**
Observed and simulated M2 lunar tide amplitudes and phases, and bias, RMSE, and relative error (RMSE/data-range) between observed and simulated sea level and velocity for each 30-day time series (including all constituents) in 2011 and 2013. Bias, the offset between simulations and observations, is defined as $Bias = \sum_1^n (x_{sim} - x_{obs})/n$ and RMSE, equivalent to the norm of the error, is defined as $RMSE = \sqrt{\sum_1^n (x_{sim} - x_{obs})^2/n}$. where $x_{sim}$, and $x_{obs}$ are the simulated and observed quantities, respectively, and $n$ is the number of independent point comparisons (approximately 240).

| | | Observations | | Simulations | | Bias | RMSE | Relative error |
|---|---|---|---|---|---|---|---|---|
| | | Amplitude | Phase | Amplitude | Phase | | | |
| **2011** | **Sea Level** | 0.18 m | 274° | 0.18 m | 240° | 0.00 m | 0.07 m | 10.5% |
| | **Velocity** | 0.58 m/s | 220° | 0.82 m/s | 198° | −0.01 m/s | 0.15 m/s | 10.1% |
| **2013** | **Sea Level** | 0.20 m | 348° | 0.16 m | 317° | 0.00 m | 0.04 m | 5.5% |
| | **Velocity** | 0.57 m/s | 217° | 0.94 m/s | 213° | 0.00 m/s | 0.10 m/s | 8.2% |

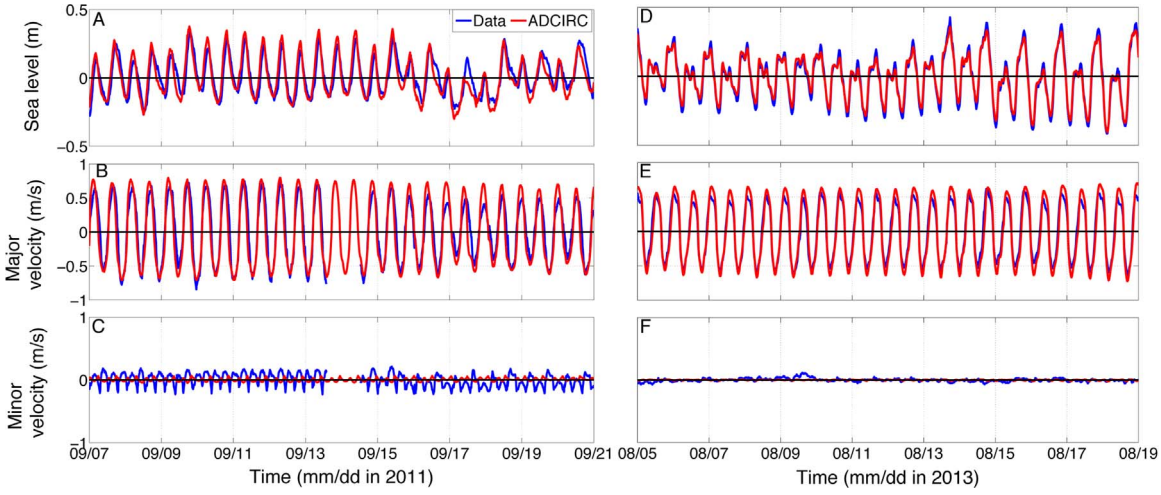


**Fig. 3.** Observed (blue curves) and modeled (red curves) (A and D) sea-surface elevation, and (B and E) major- and (C and F) minor-axis depth-averaged velocities in Katama Inlet (sensor 05, Fig. 2) versus time in 2011 (A-C) and 2013 (D-F). For sea-surface elevation fluctuations, the M2 constituent contains more than 70% of the energy. Model-data comparisons for the M2 constituent as well as biases, RMSE, and relative errors are listed in Table 1. The largest model velocity errors occur in Katama Inlet.

The model also simulates the velocities observed along the major flow axes in Katama Inlet in both 2011 (Fig. 3(B)) and 2013 (Fig. 3(E)) with errors less than about 10% (Table 1). The slight lead in the modeled sea-surface elevation fluctuations relative to the observations, and the slight overestimation of the velocity fluctuations, could be owing to an underestimation of Manning's $n$. In contrast to the reasonable model-data agreement for the major-axes flows, the model does not predict the strength of the minor-axes flows observed in Katama Inlet in 2011 (Fig. 3(C)). Although relatively weak compared with the major-axes flows, the observed minor-axes flows are stronger than predicted, possibly owing to unmodeled processes, such as alongshore propagation of the tide on the boundaries (Leeuween and DeSwart, 2002), sea breezes, or 3D effects, as well as to incorrect model bathymetry.

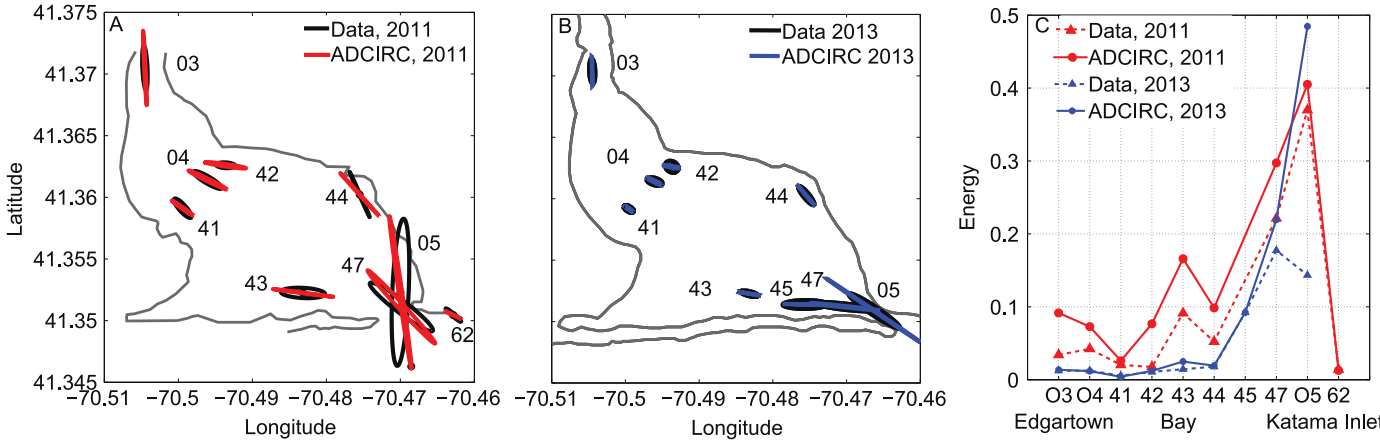


**Fig. 4.** Observed (black) and modeled (red and blue) principal flow axes in (A) 2011 (red) and (B) 2013 (blue). (C) Total velocity energy (minor-axis-velocity$^2$ + major-axis-velocity$^2$) at each sensor location versus sensor number (locations are listed near each ellipse in A and B). Triangles are observations (connected by dashed lines) and circles are model predictions (connected by solid lines). Sensor 62 was near the surfzone outside the inlet. The amplitudes of observed major-axis velocities at sensor 05 were approximately 0.6 (2011) and 0.4 (2013) m/s.

The doubling of the frequency of the observed minor-axis flows at Katama Inlet in 2011 (Fig. 3(C)) is caused by flow curvature around the spit near the sensor (Figs. 1(C) and 2(A)) that results in similar east-west components of the flow during ebb (toward south east) and during flood (toward the north east). In 2013 the inlet geometry and the sensor location differed from those in 2011, and both the observed and simulated minor-axis flows were negligible (Fig. 3(F)), possibly because the significantly longer and narrower inlet in 2013 restricted cross-channel flow.

The model simulates sea levels and currents in Edgartown Channel and throughout the Bay for both September 2011 and August 2013 (Fig. 4). Modeled major-axis flows are somewhat stronger than observed, and modeled minor-axis flows are somewhat weaker than observed (compare colored with black ellipses in Fig. 4(A), (B), and compare the circles with triangles representing the energy of the currents in Fig. 4(C)), likely owing to unmodeled processes listed above.

Observed and modeled maximum currents in Edgartown Channel and Katama Bay were significantly smaller in 2013 than in 2011 (compare ellipses in Fig. 4(A) with those in 4(B)), and the overall kinetic energy of the currents (minor-axis-velocity$^2$ + major-axis-velocity$^2$) decreased by as much as 2/3 (Fig. 4(C)). Model simulations suggest the reduction in currents from 2011 (Fig. 5(A), (B)) to 2013 (Fig. 5(C), (D)) occurs over most of the domain, except within some parts of Katama Inlet. Although the strength of the circulation decreases as the inlet evolves, the spatial patterns of the currents remain qualitatively similar during both flood and ebb flows (Fig. 5).

## 6. Discussion

Although the long-term (few years) evolution of Katama Inlet has resulted in a loss of velocity energy throughout the Katama system (Fig. 4(C)), the change has not been monotonic. For example, Hurricane Irene impacted the Katama system in late August 2011, resulting in significant changes to the inlet bathymetry, including areas with $>2$ m of erosion or accretion (Fig. 6). The model run with pre- and post-storm bathymetry and forced with the same 4-week-long time series of observed tidal levels in the sound and ocean suggests the bathymetric changes result in an increase of current speed (energy) throughout the bay (Fig. 7).

As the inlet evolved between 2011 and 2013, the tidal constituents of both the observed (Fig. 8(A)) and simulated (not shown, similar to the observations) sea-surface elevation time series in Edgartown Channel did not change significantly, and are similar to those in Vineyard Sound (not shown). In contrast, the M4 and M6 constituents of the velocity magnitude (primarily major-axis flows), as well as the ratio of these constituents to the M2 constituent, increased from 2011 to 2013 (Fig. 8(B)). The relatively larger increase in the M6 component, for both model and observations, suggests a larger role of changes in friction than in advection. The model under predicts the observed levels of the M4 and M6 velocity fluctuations (not shown), but the trend from 2011 to 2013 is similar to that observed (Fig. 8(B)).

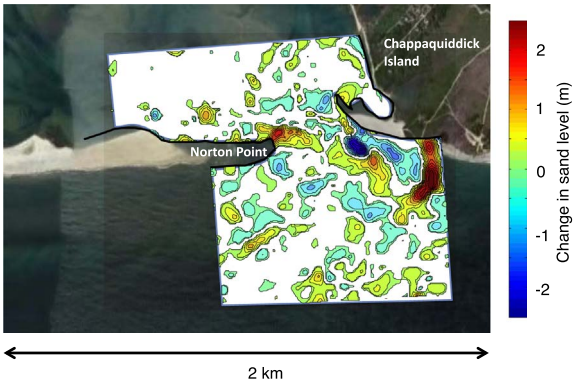


**Fig. 6.** Contours of bathymetric change between 1 month before and 1 month after the passage of Hurricane Irene, 29 Aug 2011. Red is accretion, blue is erosion (scale on the right). Changes less than 0.25 m are not shown. The inlet channel migrated eastward (to the right) and in some locations became deeper.

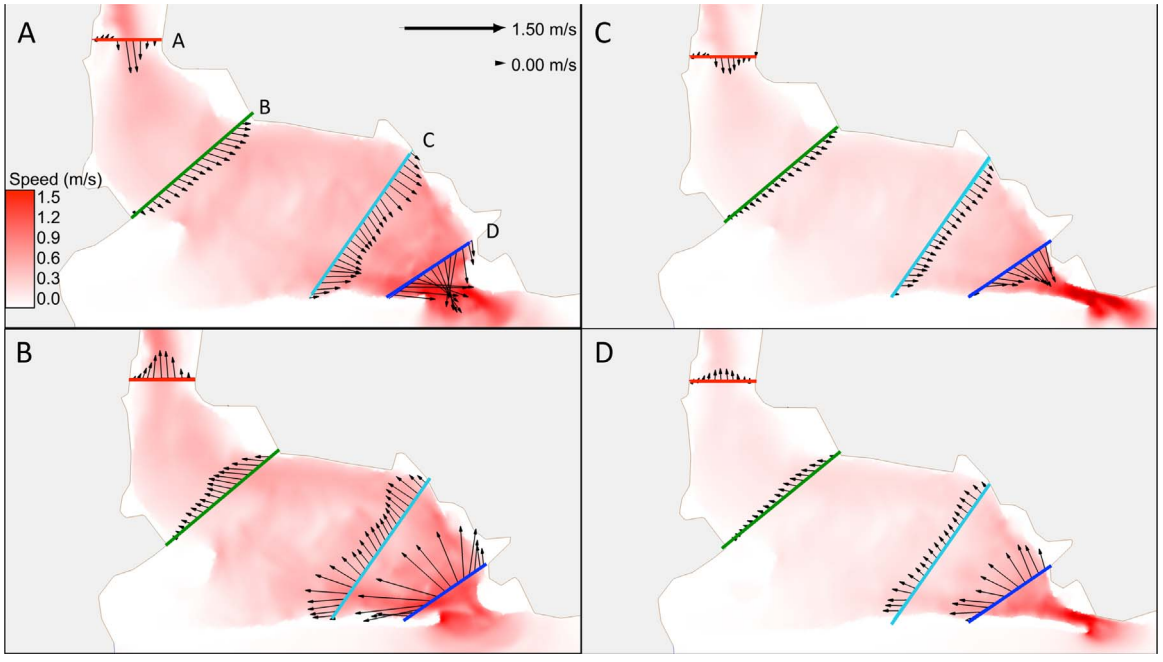


**Fig. 5.** Model simulations of velocity magnitude (color contours and length of arrows) and direction (direction of arrows) during (A and C) ebb and (B and D) flood flows in (A and B) 2011 and (C and D) 2013. Scales are shown in (A).

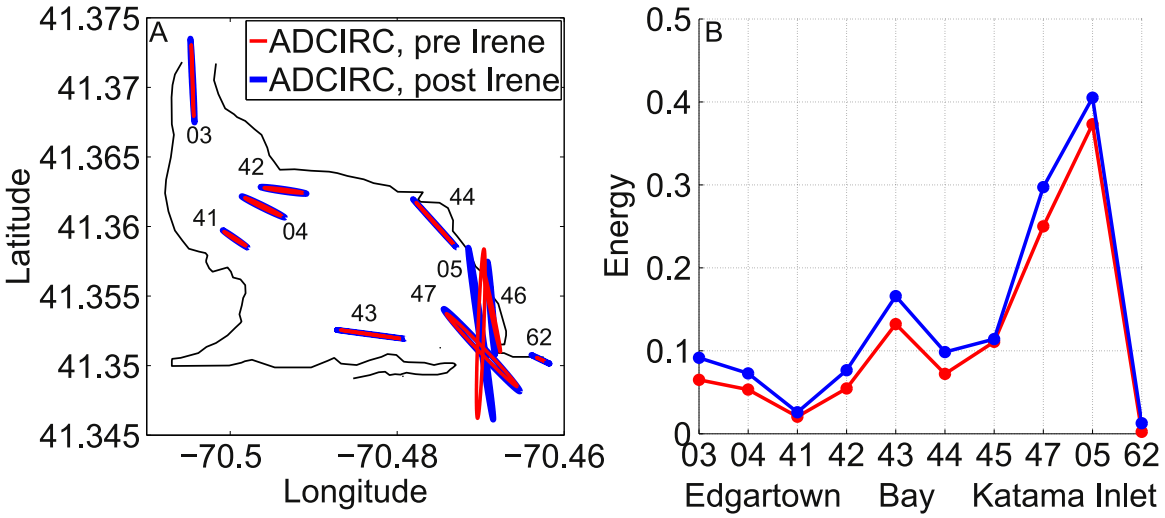


**Fig. 7.** (A) Modeled principal flow axes before (red) and after (blue) Hurricane Irene, 29 August 2011 and (B) total velocity energy (minor-axis-velocity$^2$ + major-axis-velocity$^2$) at each sensor location versus sensor number (locations are listed near each ellipse in A). Blue (pre-Irene) and red (post-Irene) lines connect predictions at the locations of the sensors. The amplitudes of major-axis velocities at sensor 05 were approximately 0.6 m/s.

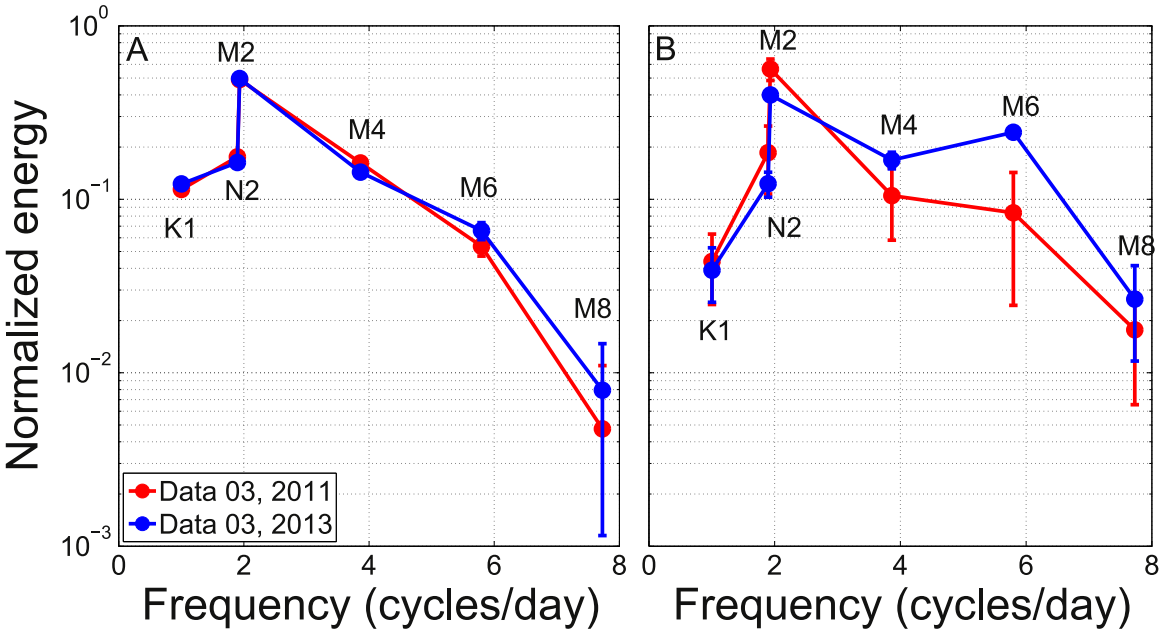


**Fig. 8.** Normalized (by the total energy) energy density versus frequency of the largest (approximately 90% of the total energy) tidal constituents from observations in Edgartown Channel (sensor 03 in Fig. 2) of (A) sea-surface elevation and (B) velocity magnitude (predominantly major-axis flow, Fig. 3). Constituent (labeled in each panel) energy and 1 standard deviation error bars were estimated using t_tide (Pawlowicz et al., 2002) from approximately 1-month long time series.

In Katama Inlet, the 2011 and 2013 M4 components of the observed and simulated (not shown) sea-surface elevation are similar to each other (compare red with blue circles in Fig. 9(A)), and are much larger than in the ocean (black in Fig. 9(A)). The relatively large M4 component, for both model and observations, suggests advection is important near the inlet. Although the M4 component of sea-surface elevation in the inlet did not change as the inlet evolved (compare red with blue in Fig. 9(A)), the M6 components of observed and simulated (not shown) sea-surface elevation are similar to those in the ocean in 2011 (compare red with black in Fig. 9(A)), and their ratio to the M2 component increases by a factor of 3 or more in 2013 (compare blue with red in Fig. 9(A)). Similar to sea-surface elevation, the M6 component of velocity at Katama Inlet increases from 2011 to 2013 (compare blue with red in Fig. 9(B)), whereas the M4 component decreases between 2011 and 2013 (Fig. 9(B)). The observed and modeled (not shown) decrease in M4 and the increase in the M6 component as the inlet evolved between 2011 and 2013 are consistent with a decreasing relative importance of advection and an increasing relative importance of friction as the inlet became longer, narrower, and shallower.

To simulate the effect of increased friction without changing the inlet geometry, the model was run with the 2011 bathymetry (wide, short, deep inlet) and boundary forcing conditions, but with Manning's $n$ increased to $n=0.085$ within Katama Inlet. The resulting circulation patterns are similar to those observed and modeled in 2013 with $n=0.035$ (Fig. 10), and are significantly less energetic than in 2011 (dashed lines in Fig. 10(B)), supporting the conclusion that the differences in circulation in the bay are primarily the result of increased friction in the 2013 inlet. The increase in frictional damping as the inlet lengthens has been hypothesized to contribute to the inlet closure (Ogden, 1974).

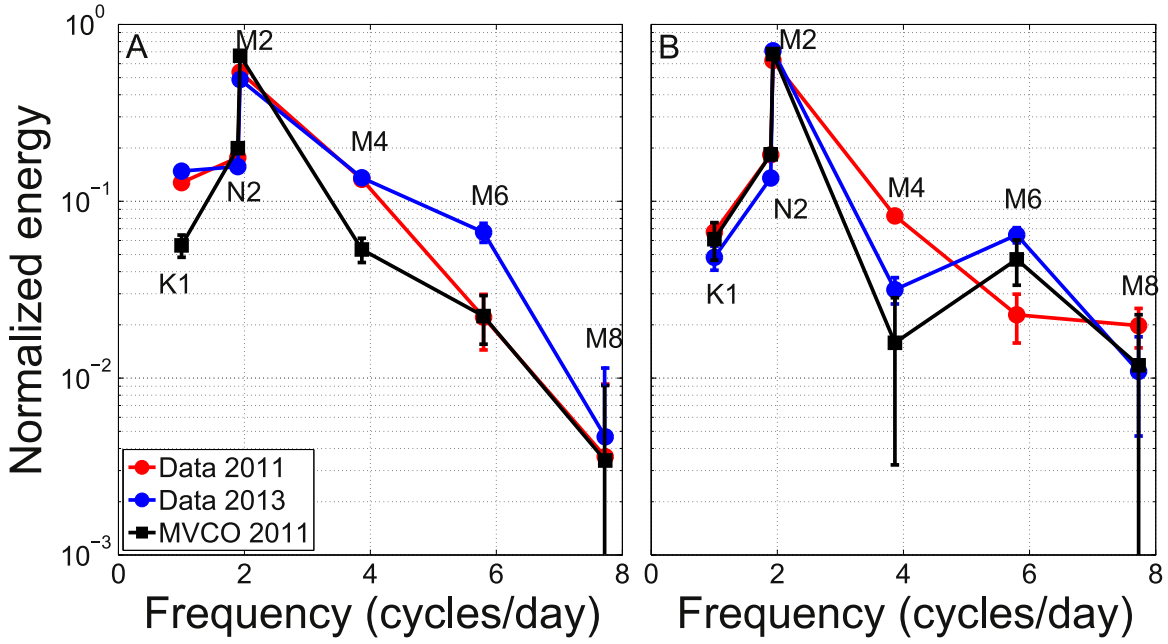


**Fig. 9.** Normalized (by the total energy) energy density versus frequency of the largest (approximately 90% of the total energy) tidal constituents from observations at the Martha's Vineyard Coastal Observatory (MVCO, black, 2011) and in Katama Inlet (sensor 05 in Fig. 2, red 2011 and blue 2013) of (A) sea-surface elevation and (B) velocity magnitude (predominantly major-axis flow, Fig. 3). Constituent (labeled in each panel) energy and 1 standard deviation error bars were estimated using t_tide (Pawlowicz et al., 2002) from approximately 1-month long time series.

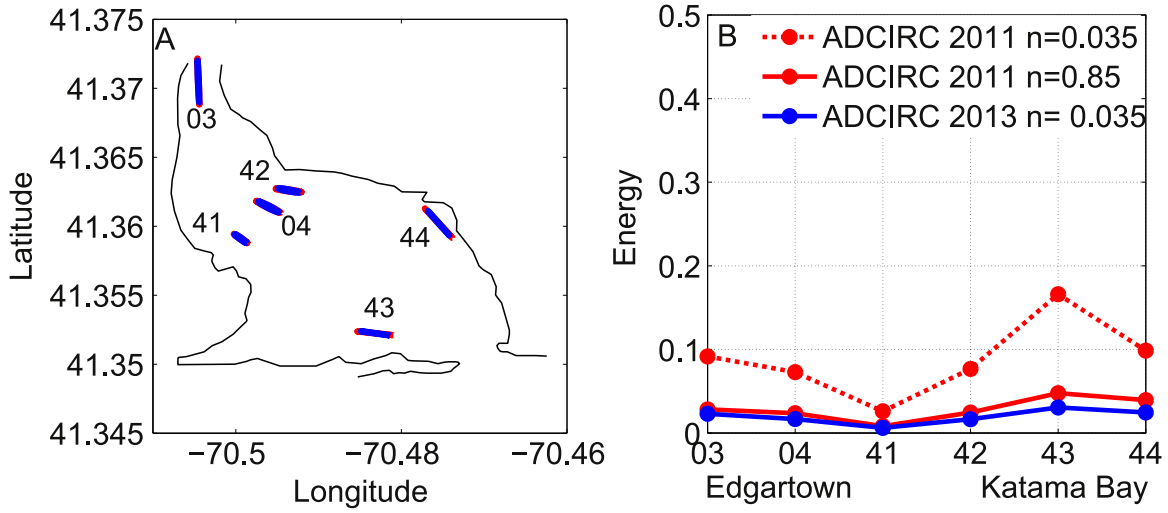


**Fig. 10.** (A) Modeled principal flow axes using the 2011 bathymetry with Manning's $n = 0.085$ (red) and the 2013 bathymetry with $n = 0.035$ (blue). Both model runs use the same boundary conditions. (B) Total velocity energy (minor-axis-velocity$^2$ + major-axis-velocity$^2$) at each sensor location versus sensor number (locations are listed near each ellipse in A). Solid red ($n$=0.085, 2011 bathymetry), blue ($n$=0.035, 2013 bathymetry), and dashed red ($n$=0.035, 2011 bathymetry) lines connect predictions at the locations of the sensors. The amplitudes of modeled major-axis velocities at sensor 03 were approximately 0.3 m/s in 2011 and 2013.

Although the tidal constituents of both velocity (Figs. 8(B) and 9(B)) and sea-surface elevation (Figs. 8(A) and 9(A)) are consistent with an increased role of friction, there are significant differences in the spectra. Unlike a single progressive wave (Aubrey and Speer, 1985; Dronkers, 1986; Friedrichs and Aubrey, 1988; Friedrichs et al., 1992; Friedrichs, 2010) or a standing wave (caused by reflection of the tide) (Broenkow and Breaker, 2005; Thornton et al., 2015), in the Katama system there are two waves propagating in opposite directions, and possibly partially reflecting and dissipating. For example, the phases between sea-surface and velocity fluctuations in the observations at M2 in 2011 and 2013 at Edgartown were 33° and −4° and at Katama were −55° and 49°, respectively (The coherence between M2 sea-surface elevation and velocity is high.). Thus, the total tide (M2 and constituents) may consist of multiple waves, and shapes of sea-surface elevation fluctuations are not necessarily related to shapes of velocity fluctuations. For example, although observed and modeled sea-surface elevation skewness [the mean of the cube of the demeaned time series normalized by the variance raised to the 3/2 power (Elgar and Guza, 1985; Nidzieko, 2010; and many others)] at Edgartown was negative in both 2011 and 2013 (not shown), implying flood dominance for the sign convention used here (Nidzieko, 2010), velocity skewness was not significantly different than 0 (not shown). Similarly, although sea-surface elevation skewness at Katama is positive in 2011 and negative in 2013 (Fig. 11(B)), implying a change from flood to ebb dominance, observed velocity skewness is not statistically different than 0 in either year (Fig. 11(C)).

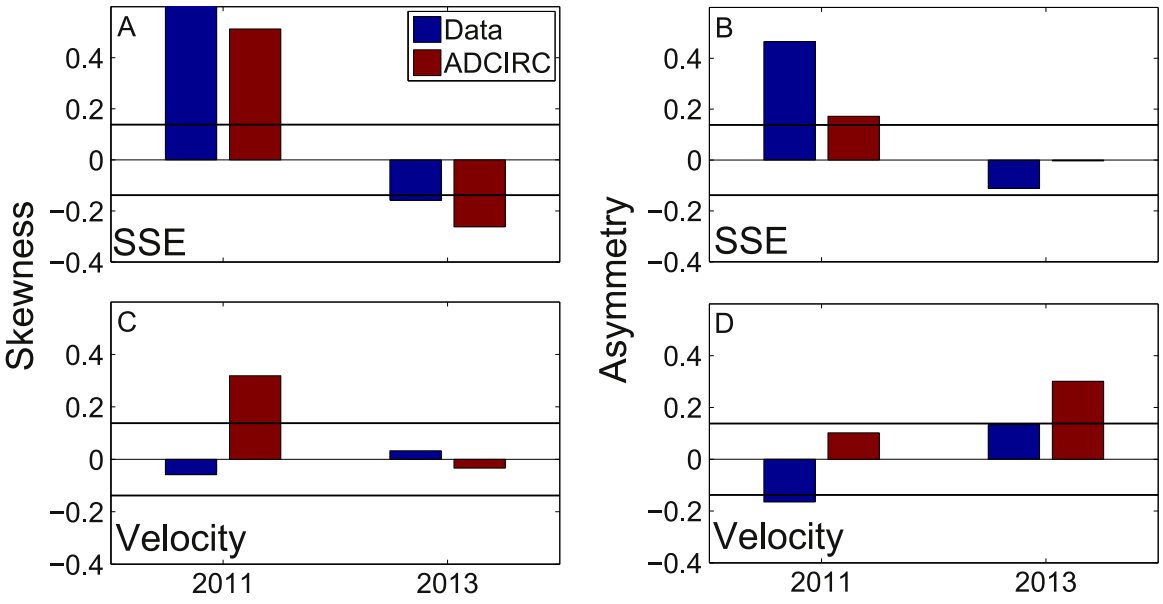


**Fig. 11.** (A and C) Skewness and (B and D) asymmetry of observed (blue) and modeled (red) sea-surface elevation (A and B) and velocity (C and D) at Katama Inlet for 2011 and 2013. For a random process with the same number of degrees of freedom as the observations, skewness and asymmetry (absolute) values greater than 0.14 (the thick horizontal lines) are statistically greater than 0 at the 90% level. Skewness is the mean of the cube of the time series normalized by the variance to the 3/2 power, and asymmetry is the mean of the cube of the Hilbert transform (a 90° phase shift) of the time series normalized by its variance to the 3/2 power.

Skewness describes asymmetries of the time series about the horizontal axis (e.g., wave crests are shaped differently than troughs). Velocities that are asymmetrical about a vertical axis (front and rear faces of the wave differ) (Kim and Powers, 1979; Masuda and Kuo, 1981; Elgar and Guza, 1985; Nidzieko, 2010) are described by the skewness of a 90° phase-shifted version (the Hilbert transform) of the time series (called "asymmetry" (Elgar and Guza, 1985), similar to the "duration skewness" (Nidzieko, 2010; Nidzieko and Ralston, 2012)). Here, sea-surface elevation and velocity asymmetry at Edgartown were not different than 0 (not shown), but at Katama sea-surface elevation asymmetry went from positive to zero (Fig. 11(B)), while velocity asymmetry went from negative to positive (Fig. 11(D)), consistent with a change from flood to ebb dominance between 2011 and 2013. Future investigation into the sediment transport within this system is necessary to address whether the observed tidal distortion and change from flood to ebb dominance plays a role in morphological changes, including inlet closure.

## 7. Conclusions

Observations and numerical simulations show that the circulation in Katama Bay became less energetic between 2011 and 2013, primarily owing to increased frictional losses as the inlet channel lengthened, narrowed, and shoaled. The model (2DDI-ADCIRC) suggests that the 2-yr trend of decreasing currents was not monotonic. For example, bathymetric changes caused by the passage of Hurricane Irene resulted in stronger modeled currents than before the hurricane. As the inlet geometry changed, the M4 harmonic (associated with advection) of the primary M2 tide did not change, while the M6 component increased, consistent with increased friction. As Katama Inlet evolved, the flows in Edgartown Channel remained flood dominant, whereas the velocity skewness and asymmetry at Katama Inlet suggest flows changed from flood to ebb dominant.

## Acknowledgements

We thank Mumen Alzubi, Kohl Brinkman, Maria Brown, David Clark, Danik Forsman, Levi Gorrell, Jeff Hansen, Sean Kilgallin, Melissa Moulton, Christen Rivera-Erick, Maddie Smith, Jenna Walker, Anna Wargula, Billy Wells, Regina Yopak, and Seth Zippel for helping to obtain the data, Janet Fredericks for help with the MVCO data, Clare Gesualdo, Charlie Blair, and the Edgartown Reading Room for providing pier pilings for pressure gauges and moorings for small boats, Mike Creato for providing staging space and a pleasant place to work at Katama Airpark, Jason Flemming for help during the ADCIRC Boot Camp, and Julia Hopkins for help with bathymetry for model grids. Two anonymous referees are thanked for their helpful comments. The Office of Naval Research, the National Science Foundation, NOAA Sea Grant, and the Office of the Assistant Secretary of Defense for Research and Engineering provided funding.

## References

Anderson, D., 2012. Sediment transport processes in a coastal lagoon: Katama Inlet, Martha's Vineyard. Senior thesis, Boston College.

Aubrey, D.G., Speer, P.E., 1985. A study of nonlinear tidal propagation in shallow inlet/ estuarine systems. Part I: Observations. Estuar. Coast. Shelf Sci. 21 (2), 185–205.

Blanton, J.O., Lin, G.Q., Elston, S.A., 2002. Tidal current asymmetry in shallow estuaries and tidal creeks. Cont. Shelf Res. 22, 1731–1743.

Breaker, L.C., Broenkow, W.W., Watson, W.E., Jo, Y.H., 2008. Tidal and nontidal oscillations in Elkhorn Slough. Ca. Est. Coast 31 (2), 239–257.

Broenkow, W.W., Breaker, L.C., 2005. A 30-year history of tide and current measurements in Elkhorn Slough, California (November 18, 2005). Scripps Inst. Ocean. Libr., 8 ⟨http://repositories.cdlib.org/sio/lib/8⟩.

Brouwer, R.L., Schuttelaars, H.M., Roos, P.C., 2013. Modelling the influence of spatially varying hydrodynamics on the cross-sectional stability of double inlet systems. Ocean Dyn. 63, 1263–1278.

Chen, C., Huang, H., Beardsley, R.C., Xu, Q., Limeburner, R., Cowles, G.W., Lin, H., 2011. Tidal dynamics in the Gulf of Maine and New England Shelf: an application of FVCOM. J. Geophys. Res. 116 (C12), C12010. http://dx.doi.org/10.1029/2011JC007054.

Dias, J.M., Sousa, M.C., Bertin, Z., Fortunato, A.B., Oliveira, A., 2009. Numerical modeling of the impact of the Ancão Inlet relocation (Ria Formosa, Portugal). Env. Model. Soft 24, 711–725.

Dronkers, J., 1986. Tidal asymmetry and estuarine morphology. Neth. J. SEA Res. 20, 117–131.

Elgar, S., Guza, R.T., 1985. Observations of bispectra of shoaling surface gravity waves. J. Fluid Mech. 161, 425–448.
Fortunato, A.B., Oliveira, A., 2005. Influence of intertidal flats on tidal asymmetry. J. Coast. Res., 21, 1062–1067.
Friedrichs, C.T., Aubrey,D.G., 1988, Non-linear tidal distortion in shallow well-mixed estuaries: a synthesis, Est. Coast. Shelf Sci. 27 (5), 521-545.
Friedrichs, C.T., Lynch, D.R., Aubrey, D.G., 1992. Velocity asymmetries in frictionally dominated tidal embayments: Longitudinal and lateral variability. In: Prandle, D. (Ed.), Dynamics and Exchanges in Estuaries and the Coastal Zone, Coastal Estuarine Stud. vol. 40. AGU, Washington, D. C, pp. 276–312.
Friedrichs, C.T., Madsen, O.S., 1992. Nonlinear diffusion of the tidal signal in frictionally dominated embayments. J. Geophys. Res. 97, 5637–5650.
Friedrichs, C.T., 1995. Stability shear stress and equilibrium cross-sectional geometry of sheltered tidal channels. J. Coast Res 11 (No. 4), 1062–1074.
Friedrichs, C.T., 2010. Barotropic tides in channelized estuaries. Contemporary Issues Estuar. Phys., 27–61.
Geyer, W.R., MacCready, P., 2014. The estuarine circulation. Ann. Rev. Fluid Mech. 46, 175–197.
Keulegan, G.H., 1967. Tidal Flow in entrances; Water-Level fluctuations of Basins in Communication with Seas (No. Cth Technical Bulletin-14). Committee on Tidal Hydraulics (Army) Washington DC.
Kim, Y.C., Powers, E.J., 1979. Digital bispectral analysis and its application to nonlinear wave interactions. IEEE Trans. Plasma Sci. 7, 120–131.
Kraus, N.C., Militello, A., 1999. Hydraulic study of multiple inlet system: East Matagorda Bay, Texas. J. Hydraul. Eng. 125, 224–232.
Luettich, R.A., Westerink, J.J., 1991. A solution for the vertical variation of stress, rather than velocity, in a three-dimensional circulation model. Int. J. Numer. Method Fluid 12, 911–928.
MacCready, P., Geyer, W.R., 2010. Advances in estuarine physics. Ann. Rev. Mar. Sci. 2, 35–58.
Malhadas, M., Leitao, P., Silva, A., Neves, R., 2009. Effect of coastal waves on sea level in Obidos Lagoon, Portugal. Cont. Shelf Res. 29, 1240–1250.
Masuda, A., Kuo, Y.-Y., 1981. A note on the imaginary part of bispectra. Deep-SEA Res. 28, 213–222.
Mehta, A.J., Joshi, P.B., 1988. Tidal inlet hydraulics. J. Hydraul. Eng. 117, 1321–1338.
Nidzieko, N.J., 2010. Tidal asymmetry in estuaries with mixed semidiurnal/diurnal tides. J. Geophys. Res. 115, C08006. http://dx.doi.org/10.1029/2009JC005864.
Nidzieko, N.J., Ralston, D., 2012. Tidal asymmetry and velocity skew over tidal flats and shallow channels within a macrotidal river delta. J. Geophys. Res. 117, C03001. http://dx.doi.org/10.1029/2011JC007384.
Ogden, J., 1974. Shoreline changes along the southeastern coast of Martha's Vineyard, Massachusetts for the past 200 years. Quart. Res., 4.
Orescanin, M., Raubenheimer, B., Elgar, S., 2014. Observations of wave effects on inlet circulation. Cont. Shelf Res. 82, 37–42.
Parker, B.B., 1991. The relative importance of the various nonlinear mechanisms in a wide range of tidal interactions (Review). In: Parker, B.B. (Ed.), Tidal Hydrodynamics. John Wiley & Sons, New York.
Pawlowicz, R., Beardsley, B., Lentz, S., 2002. Classical tidal harmonic analysis including error estimates in MATLAB using T_TIDE. Comput. Geosci. 28, 929–937.
Prandle, D., 1991. Tides in estuaries and embayments. In: Parker, B.B. (Ed.), Tidal Hydrodynamics. John Wiley & Sons, New York.
Speer, P.E., Aubrey, D.G., 1985. A study of nonlinear tidal propagation in shallow inlet/ estuarine systems. Part II: Theory. Est. Coast. Shelf Sci. 21 (2), 207–224.
Speer, P., Aubrey, D.G., Friedrichs, C.T., 1991. Nonlinear hydrodynamics of shallow tidal inlet/bay systems. In: Parker, B.B. (Ed.), Tidal Hydrodynamics. John Wiley & Sons, New York.
Thornton, E., MacMahan, J., Elgar, S., Gon, C., Reniers, A., 2015. Tidal wave reflection and asymmetry in a short estuary. J. Geophys. Res., submitted.
Van de Kreeke, J., Brouwer, R.L., Zitman, T.J., Schuttelaars, H.M., 2008. The effect of a topographic high on the morphological stability of a two-inlet bay system. Coast. Eng. 55 (4), 319–332.
Wargula, A., Raubenheimer, B., Elgar, S., 2014. Wave-driven along-channel subtidal flows in a well-mixed ocean inlet. J. Geophys. Res.: Ocean. 119 (5), 2987–3001.